Soft Matter

PAPER

View Article Online
View Journal | View Issue

Cite this: *Soft Matter*, 2023, **19**, 2832

Liquid structure of bistable responsive macromolecules using mean-field density-functional theory

Arturo Moncho-Jordá, *[ab] Nils Göth [c] and Joachim Dzubiella *[c]

Received 21st November 2022,
Accepted 16th March 2023

DOI: 10.1039/d2sm01523d

rsc.li/soft-matter-journal

Macromolecular crowding typically applies to biomolecular and polymer-based systems in which the individual particles often feature a two-state folded/unfolded or coil-to-globule transition, such as found for proteins and peptides, DNA and RNA, or supramolecular polymers. Here, we employ a mean-field density functional theory (DFT) of a model of soft and bistable responsive colloids (RCs) in which the size of the macromolecule is explicitly resolved as a degree of freedom living in a bimodal 'Landau' energy landscape (exhibiting big and small states), thus directly responding to the crowding environment. Using this RC-DFT we study the effects of self-crowding on the liquid bulk structure and thermodynamics for different energy barriers and softnesses of the bimodal energy landscape, in conditions close to the coil-to-globule transition. We find substantial crowding effects on the internal distributions, a complex polydispersity behavior, and quasi-universal compression curves for increasing (generalized) packing fractions. Moreover, we uncover distinct signatures of bimodal *versus* unimodal behavior in the particle compression. Finally, the analysis of the pair structure – derived from the test particle route – reveals that the microstructure of the liquid is quite inhomogeneous due to local depletion effects, tuneable by particle softness.

1 Introduction

The phenomenon of macromolecular crowding in biomolecular and polymer-based systems has attracted great attention during the last decades due to its huge implications on the macromolecular structure, stability, as well as conformational transitions and dynamics.[1–7] All these properties have profound implications on (bio)chemical reactions in physiological or synthetic media.[8] Indeed, biological macromolecules have evolved and function within intracellular environments that are surrounded by other macromolecules at large concentrations. Within these crowded environments, the interactions between macromolecules become substantial, driven not only by volume exclusion effects, but also by other nonspecific interactions, such as electrostatics and hydrophobicity.[3,9,10] Better understanding of the mechanisms and consequences of molecular crowding is not only of fundamental and biological interest but will improve the design of functional materials, *e.g.*, synthetic cellular nanosystems.[11]

Theoretical studies of macromolecular crowding usually assume that the macromolecules are hard and stiff entities, and have no internal degrees of freedom (DoFs). However, due their polymeric nature the particles feature large conformational behavior and rather behave in many cases effectively as soft and responsive, and so are able to modify their effective size in response to the external stimuli. For instance, organelle sizes inside the cell fluctuate in demand, swelling or shrinking, to preserve the cell homeostasis,[12] and soft and compressible lipid vesicles undergo compaction by increasing the concentration of high molecular weight PEG-based crowders.[13]

Furthermore, the conformation of biological or functional macromolecules often displays a two-state behavior, such as in folded/unfolded or globule/coil transitions of proteins and polymers.[5,14–19] Crowding leads to a restriction of the available space that usually promotes the folded (deswollen or globular) state.[5,7,20] Simple models to explain two-state behavior are either based on discrete state models[14–16] or on continuous bistable Landau-like models.[21,22] However, the consequences of bimodal behavior on the systems' bulk structure and compression behavior are not well understood. In particular, playing with particle softness/stiffness (defined as a measure of how easily the particle size changes under pressure) and particle

[a] *Institute Carlos I for Theoretical and Computational Physics, Facultad de Ciencias, Universidad de Granada, Campus Fuentenueva S/N, 18071 Granada, Spain. E-mail: moncho@ugr.es*
[b] *Departamento de Física Aplicada, Universidad de Granada, Campus Fuentenueva S/N, 18071 Granada, Spain*
[c] *Physikalisches Institut, Albert-Ludwigs-Universität Freiburg, Hermann-Herder Straße 3, D-79104 Freiburg, Germany. E-mail: joachim.dzubiella@physik.uni-freiburg.de*

hardness (defined as a measure of the interparticle penetrability) is expected to allow fine control and tuneability of the bulk structure and thermodynamics, but is yet unexplored.

In this work, we consider systems formed by identical bistable macromolecular species, each modeled by soft repulsive spheres with a generic Landau-like bimodal size distribution.[21,22] We employ the model of 'Responsive Colloids' (RCs) where an internal DoF (here, the particle size, σ) is explicitly resolved in an one-body contribution to the Hamiltonian, defining an internal 'parent' energy landscape, $\psi(\sigma)$.[23] σ represents an internal coarse-grained property of the particle that is explicitly altered by the environment and particle–particle interactions. The RC model has already been applied, *e.g.*, to study the equilibrium structure and dynamics of unimodal, elastic ('Hertzian') colloids in bulk using overdamped Brownian dynamics (BD) simulations.[24] The polydispersity in such a model is dynamical, and interesting many-body correlations and novel diffusion effects were uncovered, some in line with earlier Monte-Carlo simulations of explicitly compressible microgels.[25] Moreover, using a bimodal parent landscape of the colloidal size, the influence of crowding on the internal switching kinetics was examined using BD simulations.[26] However, the explicit effects of particle softness and hardness on particle's mean size, polydispersity, packing fraction and other structural bulk properties have not been systematically considered. In addition, it would be desirable to have complementary theoretical tools than BD simulations to study the structure and thermodynamics of larger systems in equilibrium and nonequilibrium more efficiently.[27]

For these purposes, we combine the RC model with classical density-functional theory (DFT), which is a powerful machinery to efficiently describe the structure and thermodynamics of liquids.[28] In equilibrium, the RC model is equivalent to conventional polydisperse systems in the thermodynamic limit,[23] for which DFT was successfully constructed.[29,30] We note that the research of polydisperse systems surprisingly calmed down, and studies beyond hard spheres with simple unimodal Gaussian parents have been rare since. As a noteworthy exception, Schmidt and Denton showed, using DFT of models of colloid–polymer mixtures which resolved the polymer size as an explicit DoF, how crowding leads to polymer compression and shifts the demixing fluid binodal compared to incompressible systems.[31] Here, we adapt and extend these methods in accordance with our bistable RC model and solve it for soft, Gaussian pair potentials assuming a mean-field approximation for the inhomogeneous free energy functional. The RC-DFT machinery is then employed to study bulk structure, polydispersity, and pressure systematically for different forms of the bimodal energy landscape characterized by its energy barrier and its softness. By comparing to the unimodal case (no bistability),[24,25] we find large differences for the bistable colloids and some key signatures of bistability in the compression curves.

Our model is sufficiently generic to describe the qualitative behavior of a wide range of crowded soft systems and represents a first approximation to describe conformational (coil-to globule) transitions of globular proteins and peptides having two (*e.g.*, folded/unfolded) conformations,[32,33] including intrinsically disordered proteins[17] or synthetic supramolecular polymers,[18] but also DNA or RNA chains,[5,19] and prototypical thermosensitive polymers.[34–36]

The paper is organized as follows. In Section 2 we introduce the theory and present the main DFT mean-field equations required to determine the one-body density profile, the local size distribution and the microstructure of the RC model (Section 3). We complement our numerical DFT study with perturbation theory described in Section 4. Then, in Section 5 we apply this theoretical framework to investigate how particle squeezing modifies the particle size and volume distribution, the packing fraction, polydispersity, osmotic pressure, as well as the colloidal microstructure (pair distribution functions) of the homogeneous RC systems. We close with a brief summary, concluding remarks, and an outlook on worthwhile future work.

2 Theory

2.1 Distributions of responsive colloids

In ordinary DFT, the equilibrium properties of a non-responsive colloidal system immersed in an external potential, $u_{\text{ext}}(\mathbf{r})$, are determined by the inhomogeneous one-body density profile, $\rho(\mathbf{r})$, where $\mathbf{r}$ is the particle position. Integration over the entire volume V of the system gives the total number of particles, $\int_V \rho(\mathbf{r})\mathrm{d}\mathbf{r} = N$. This framework assumes that the particles forming the system do not have any internal DoFs.

In the more general case of responsive colloids (RCs), the size of the colloids (σ) changes in response to the interactions with other particles or with an applied external potential. In addition, this external field not only depends on position, but also it could vary with the particle size, *i.e.* $u_{\text{ext}}(\mathbf{r},\sigma)$. In other words, the external potential makes the colloidal system inhomogeneous in terms of position and also size distribution. Therefore, we have to consider the joint distribution of the particle position and size, $\rho(\mathbf{r},\sigma)$. In the following we briefly recall the most basic statistical relations between distributions and means.[23]

Integration over the four coordinates provides the total number of particles,

$$\int_V \mathrm{d}\mathbf{r} \int \mathrm{d}\sigma \rho(\mathbf{r},\sigma) = N \tag{1}$$

so $\rho(\mathbf{r},\sigma)$ is measured in units of length^{-4}. In the absence of an external field, the system becomes homogeneous. In addition, in the limit of very low particle concentrations, the one-body density can be written as

$$\lim_{\rho_0 \to 0} \lim_{u_{\text{ext}} \to 0} \rho(\mathbf{r},\sigma) = \rho_0 p(\sigma) \tag{2}$$

where $\rho_0 = N/V$ is the bulk number density, and $p(\sigma)$ is the single-particle probability distribution of size, which is normalized to unity, $\int p(\sigma)\mathrm{d}\sigma = 1$. Hence, $p(\sigma)$ is the size distribution of a single isolated responsive particle that does not interact with external forces or with other particles. We can express $p(\sigma)$ as

$$p(\sigma) = p_0 \mathrm{e}^{-\beta\psi(\sigma)}, \tag{3}$$

where $\beta^{-1} = k_B T$ (T is the absolute temperature and k_B the Boltzmann constant) and $\psi(\sigma)$ is the corresponding free-energy landscape. It represents a coarse-grained conformational free energy of the particle, *i.e.*, the energy cost associated with swelling of shrinking the particle size. p_0 is a constant prefactor required to fulfill the normalization of $p(\sigma)$. We will call $p(\sigma)$ the *parent* size distribution.

If the particle concentration is increased beyond the dilute regime and/or the external potential u_{ext} is turned on, interactions with the surrounding particles and with the external potential will affect this single-particle property distribution. We denote by $f(\sigma) = N(\sigma)/N$ the emergent probability distribution, where $N(\sigma)d\sigma$ is the number of particles with internal property within $[\sigma,\sigma + d\sigma]$ in the system. In particular, in the absence of any external field, we have

$$\lim_{u_{ext}\to 0} \rho(\mathbf{r},\sigma) = \rho_0 f(\sigma) = \rho_0 \frac{N(\sigma)}{N} \tag{4}$$

Integration of $\rho(\mathbf{r},\sigma)$ leads to partial distribution functions. Integrating over the σ-space provides the one-body number density distribution of the RC fluid,

$$\int d\sigma \rho(\mathbf{r},\sigma) = \rho(\mathbf{r}) \tag{5}$$

The position dependent mean size is given by

$$\langle \sigma(\mathbf{r}) \rangle = \frac{1}{\rho(\mathbf{r})} \int d\sigma \rho(\mathbf{r},\sigma)\sigma \tag{6}$$

In a similar way, integrating over the volume V we obtain the size distribution

$$\int_V d\mathbf{r} \rho(\mathbf{r},\sigma) = N(\sigma) \tag{7}$$

Finally, the position-dependent size distribution is

$$f(\mathbf{r},\sigma) \equiv \frac{N(\mathbf{r},\sigma)}{N} = \frac{\rho(\mathbf{r},\sigma)}{\rho(\mathbf{r})} \tag{8}$$

$f(\mathbf{r},\sigma)$ is normalized to 1, *i.e.*, $\int f(\mathbf{r},\sigma)d\sigma = 1$, and provides the local size distribution at position $\mathbf{r}$. Its knowledge allows to measure the effect of the applied external potential $u_{ext}(\mathbf{r},\sigma)$ on the size distribution locally.

2.2 Density functional theory of a RC fluid

Let us consider a RC fluid immersed in the external potential, $u_{ext}(\mathbf{r},\sigma)$. In the same way, the particle–particle pair potential not only depends on the positions $\mathbf{r}$ and $\mathbf{r}'$ of both particles, but also has explicit dependence on the size of both interacting particles, σ and σ', that is $u(\mathbf{r},\mathbf{r}';\sigma,\sigma')$.

The inhomogeneous free energy functional of a RC fluid can be written as[23,30]

$$\begin{aligned} F[\rho(\mathbf{r},\sigma)] &= k_B T \int d\mathbf{r} \int d\sigma \rho(\mathbf{r},\sigma)\left[\ln\left(\rho(\mathbf{r},\sigma)\Lambda^3/p_0\right) - 1\right] \\ &+ \int d\mathbf{r} \int d\sigma \rho(\mathbf{r},\sigma)[u_{ext}(r,\sigma) + \psi(\sigma)] \\ &+ F_{ex}[\rho(\mathbf{r},\sigma)] \end{aligned} \tag{9}$$

where $\Lambda = h/(2\pi m k_B T)^{1/2}$ is the thermal wavelength. The first term of eqn (9) is the ideal gas free-energy functional. The second term takes into account the interaction of the RC fluid with the external potential. Note that $\psi(\sigma)$ can be viewed as an additional external potential for the particle property σ.[23] Finally, the third contribution represents the excess free energy of the fluid due to the existence of particle–particle interactions.

The grand canonical potential energy functional of a RC fluid is

$$\Omega[\rho(\mathbf{r},\sigma)] = F[\rho(\mathbf{r},\sigma)] - \mu_0 \int d\mathbf{r} \int d\sigma \rho(\mathbf{r},\sigma) \tag{10}$$

where μ_0 is the (constant) chemical potential of the RC fluid.

The equilibrium density profile is the one that minimizes the grand canonical functional

$$\frac{\delta\Omega}{\delta\rho(\mathbf{r},\sigma)} = 0 \tag{11}$$

Applying this functional differentiation to eqn (10) and using eqn (9) leads to the so-called Euler–Lagrange equation

$$k_B T \ln(\rho(\mathbf{r},\sigma)\Lambda^3/p_0) + u_{ext}(\mathbf{r},\sigma) + \psi(\sigma) + \mu_{ex}(\mathbf{r},\sigma) - \mu_0 = 0 \tag{12}$$

where the excess chemical potential $\mu_{ex}(\mathbf{r},\sigma)$ is obtained from the functional differentiation of the excess free energy

$$\mu_{ex}(\mathbf{r},\sigma) \equiv \frac{\delta F_{ex}}{\delta\rho(\mathbf{r},\sigma)} \tag{13}$$

Solving eqn (12) for the particle density $\rho(\mathbf{r},\sigma)$, we find

$$\rho(\mathbf{r},\sigma) = \frac{e^{\beta\mu_0} p_0}{\Lambda^3} \exp(-\beta\psi(\sigma) - \beta u_{ext}(\mathbf{r},\sigma) - \beta\mu_{ex}(\mathbf{r},\sigma)) \tag{14}$$

The prefactor $q = e^{\beta\mu_0}/\Lambda^3$ is a constant number with the dimensions of length^{-3}. Using eqn (3) for the single-particle distribution property $p(\sigma)$ (which is assumed to be known) we finally find

$$\rho(\mathbf{r},\sigma) = q p(\sigma) \exp(-\beta u_{ext}(\mathbf{r},\sigma) - \beta\mu_{ex}(\mathbf{r},\sigma)) \tag{15}$$

The constant q can be calculated by normalization of the density profile

$$\int d\mathbf{r} \int d\sigma \rho(\mathbf{r},\sigma) = N \tag{16}$$

Eqn (15) and (16) must be solved iteratively until convergence is achieved, leading to the equilibrium position and size distribution $\rho_{eq}(\mathbf{r},\sigma)$.

2.3 Mean-field approximation

Although the exact expression of F_{ex} is typically unknown, it is confirmed that the mean-field approximation works quite well for a wide range of bounded potentials representing soft colloids, such as linear polymer chains, dendrimers, star polymers or polyelectrolyte stars, becoming more accurate when increasing the particle density.[37,38] The mean-field excess free energy functional is given by

$$F_{ex} = \frac{1}{2}\iint d\mathbf{r}\, d\mathbf{r}' \iint d\sigma\, d\sigma' \rho(\mathbf{r},\sigma)\rho(\mathbf{r}',\sigma')u(\mathbf{r},\mathbf{r}';\sigma,\sigma') \quad (17)$$

Performing the functional differentiation leads to the explicit expression of the excess chemical potential

$$\mu_{ex}(\mathbf{r},\sigma) = \int d\mathbf{r}' \int d\sigma' \rho(\mathbf{r}',\sigma')u(\mathbf{r},\mathbf{r}';\sigma,\sigma') \quad (18)$$

Therefore, given the total number of particles in the system, N, the equilibrium one-body density profile of the mean-field RC is obtained by solving the following set of equations

$$\begin{aligned}\rho(\mathbf{r},\sigma) &= qp(\sigma)\exp(-\beta u_{ext}(\mathbf{r},\sigma)) \\ &\quad \times \exp\left(-\int d\mathbf{r}' \int d\sigma' \rho(\mathbf{r}',\sigma')\beta u(\mathbf{r},\mathbf{r}';\sigma,\sigma')\right) \\ N &= \int d\mathbf{r} \int d\sigma \rho(\mathbf{r},\sigma).\end{aligned} \quad (19)$$

Since for spherical colloids the pair interaction potential between particles depends on their relative distance, *i.e.* $u(\mathbf{r},\mathbf{r}';\sigma,\sigma') = u(|\mathbf{r} - \mathbf{r}'|;\sigma,\sigma')$, eqn (19) involves a convolution integral over the position coordinate.

To determine the equilibrium density profiles with a finite particle concentration ρ_0 as input parameter, eqn (19) is solved numerically starting from the uniform distribution $\rho(\mathbf{r},\sigma)|_0 = \rho_0 p(\sigma)$. For this purpose, this initial guess is inserted into the convolution integral of eqn (19) and then normalized $\left(\iint \rho(\mathbf{r},\sigma) d\mathbf{r}\, d\sigma = N\right)$ to calculate the next iteration, $\rho(\mathbf{r},\sigma)|_1$. This iterative procedure is repeated to obtain further interactions, n. In order to improve the stability of the method, the new solution is mixed with the old one, as $\rho(\mathbf{r},\sigma)|_{n+1} = \alpha\rho(\mathbf{r},\sigma)|_{n+1} + (1 - \alpha)\rho(\mathbf{r},\sigma)|_n$, with $\alpha = 0.1$. We consider that the procedure has converged to the final equilibrium distribution when $\iint |\rho(\mathbf{r},\sigma)|_n - \rho(\mathbf{r},\sigma)|_{n-1}|^2 d\mathbf{r}\, d\sigma < 10^{-20}$. The $\mathbf{r}$ and σ-space are both discretized in intervals of $10^{-2}\sigma_0$.

In the particular of considering a homogeneous bulk suspension of RCs (without any applied external field) eqn (19) take the form

$$\rho_0 f(\sigma) = qp(\sigma)\exp\left(-\rho_0 \int d\mathbf{r}' \int d\sigma' f(\sigma')\beta u(\mathbf{r},\mathbf{r}';\sigma,\sigma')\right), \quad (20)$$

which has to be solved with the normalization condition $\int f(\sigma) d\sigma = 1$.

2.4 Generalized radial distribution functions (RDFs)

The distribution functions that characterize the microstructure of a dispersion can be also generalized for the RC fluid. In particular, the two-body distribution function is defined as[23]

$$\rho^{(2)}(\mathbf{r},\mathbf{r}';\sigma,\sigma') = \left\langle \sum_{i=1}^{N}\sum_{j=1}^{N} \delta(\mathbf{r} - \mathbf{r}_i)\delta(\mathbf{r}' - \mathbf{r}_j)\delta(\sigma - \sigma_i)\delta(\sigma' - \sigma_j) \right\rangle \quad (21)$$

It provides the conditional probability to find a particle with property σ' located at $\mathbf{r}'$ if the other one, with property σ, is located at $\mathbf{r}$. The corresponding pair distribution function can be defined as in standard liquid state theory

$$g^{(2)}(\mathbf{r},\mathbf{r}';\sigma,\sigma') \equiv \frac{\rho^{(2)}(\mathbf{r},\mathbf{r}';\sigma,\sigma')}{\rho(\mathbf{r},\sigma)\rho(\mathbf{r}',\sigma')} \quad (22)$$

If the system is homogeneous and isotropic, then $\rho(\mathbf{r},\sigma) = \rho_0 f(\sigma)$ and the pair distribution depends only on the distance between particles, so we can define the radial pair–property distribution function $g(r;\sigma,\sigma')$, where r represents the distance between both RCs.

A powerful procedure to obtain $g(r;\sigma,\sigma')$ can be developed by making use of the Test Particle Route (TPR).[39,40] Within this method, a test particle of size σ' is fixed at the origin $r = 0$. This central particle acts as an external potential for the RC fluid, so $u_{ext}(\mathbf{r},\sigma) = u(\mathbf{r};\sigma,\sigma')$, where r here represents the distance to the test particle. Solving iteratively the mean-field DFT expression given by eqn (19) with this external potential provides the resulting equilibrium density profile of the RCs around the central test particle, $\rho(\mathbf{r},\sigma)|_{\sigma'}$. Rewriting eqn (19) for the particular case radial symmetry we find

$$\begin{aligned}\rho(r,\sigma)|_{\sigma'} &= qp(\sigma)\exp(-\beta u(r,\sigma,\sigma') - \beta\mu_{ex}(r,\sigma)) \\ N &= 4\pi \int d\sigma \int_0^R r^2 \rho(r,\sigma) dr\end{aligned} \quad (23)$$

From this density profile, we can extract the RDF as $\rho(r,\sigma)|_{\sigma'} = \rho_0 f(\sigma) g(r;\sigma,\sigma')$. Using this method, the radial pair–property distribution functions $g(r;\sigma,\sigma')$ can be calculated as

$$g(r;\sigma,\sigma') = \frac{\rho(r,\sigma)|_{\sigma'}}{\rho_0 f(\sigma)} \quad (24)$$

It can be shown that, for large values of r, $g(r;\sigma,\sigma') \to 1$. In addition, for a very diluted system, we obtain

$$\lim_{\rho_0 \to 0} g(r;\sigma,\sigma') = \exp(-\beta u(r,\sigma,\sigma')). \quad (25)$$

where we emphasize again that in the TPR method the external potential is given by the pair potential exerted by a test particle of size σ' located at $r = 0$.

To perform the TPR calculation, we chose a sufficiently large cavity of radius $R = 16\sigma_0$ and confine the RC fluid inside. This value of the radius is large enough to guarantee that $\rho(r)$ is uniform at the middle distance from the center of the cavity, $r = R/2$. Then, the total number of RC particles was selected in order to obtain the desired particle density $\rho(r = R/2) = \rho_0$.

3 RC model

We apply the mean-field DFT to investigate the compression effects of an interacting fluid of bistable RCs in bulk solution and investigate its microstructure making use of the TPR described above. We now define our specific RC model.

In all cases, to model two-state behavior, we choose a generic bimodal form of the explicit double-Gaussian function

$$p(\sigma) = \frac{A}{2\sqrt{2\pi\tau^2}}\left[\exp\left(-\frac{(\sigma-\sigma_1)^2}{2\tau^2}\right) + \exp\left(-\frac{(\sigma-\sigma_2)^2}{2\tau^2}\right)\right] \quad (26)$$

with $\sigma_1 = 0.63\sigma_0$ and $\sigma_2 = 1.37\sigma_0$, where σ_0 represents the reference particle size, that will be used as unit length for all sizes and distances ($\sigma_0 = 1$). In order to avoid nonphysical negative values and extremely large values of the particle size, the range of σ has been limited to be $\sigma \in [0,2\sigma_0]$. To satisfy the normalization condition for $p(\sigma)$, we have included in eqn (26) a corrective dimensionless prefactor A such that $\int_0^\infty p(\sigma)\mathrm{d}\sigma = 1$.

At this point, it is important to explain the physical meaning of the parameter τ. For this purpose, we show in Fig. 1 both, $p(\sigma)$ and the corresponding elastic free-energy landscape, $\psi(\sigma)$, for $\tau = 0.1\sigma_0$ and $\tau = 0.2\sigma_0$. As observed, τ provides the thickness of the size distribution. From the perspective of the energy landscape, decreasing τ leads to a sharper energy landscape and to a larger energy barrier separating the two potential wells located at σ_1 and σ_2. Therefore, τ provides an estimate of the particle softness (conversely, τ^{-1} represents the stiffness of the RC). In other words, the energy cost of compressing a RC is larger for small τ.

In order to study how bimodality affects the compression effects, we also explore RCs that follow an unimodal Gaussian distribution, defined as

$$p_{\mathrm{gauss}}(\sigma) = \frac{A}{\sqrt{2\pi\tau^2}}\exp\left(-\frac{(\sigma-\sigma_0)^2}{2\tau^2}\right), \quad (27)$$

which could also describe bistable macromolecules, but in environmental conditions (or temperatures) far away from the coil-to-globule transition, so that all of them are in only one of the two states: folded or unfolded.[41,42]

We focus in our work on systems composed by soft interpenetrable responsive spherical colloids, for which we assume the following size-dependent Gaussian pair potential for the particle–particle pair interaction

$$\beta u(\mathbf{r},\mathbf{r}';\sigma,\sigma') = \varepsilon\exp(-4|\mathbf{r}-\mathbf{r}'|^2/(\sigma+\sigma')^2), \quad (28)$$

where $|\mathbf{r}-\mathbf{r}'|$ is the distance between the centers of both particles, and σ and σ' are the particle sizes of the both interacting colloids, so that $(\sigma+\sigma')$ plays the role of the interaction range. In fact, σ represents in this interaction model the effective diameter of the colloids. $\varepsilon > 0$ is the interparticle repulsion strength, which represents a measurement of the hardness of the RCs.

The choice of the Gaussian pair potential represents a good approximation of the effective interaction between the centers of mass of ultrasoft colloids such as linear polymers chains and dendrimers.[37,43–48] The equilibrium properties of soft Gaussian particles described by eqn (28) are well represented by a weakly correlated mean-field fluid over a surprisingly wide density and temperature range, being more accurate for increasing particle densities.[37] In addition, the accuracy of mean-field DFT approach for bistable systems has been recently probed comparing the theoretical predictions for (active) two-state switching Gaussian colloids to reactive Brownian Dynamics simulation, finding good quantitative agreement.[49–51]

Note that the hardness ε and the stiffness τ^{-1} are typically not independent quantities, as stiffer colloids also repel each other more strongly. However, in order to investigate the role of both parameters, we treat ε and τ as independent variables. In particular, the calculations were performed choosing $\varepsilon = 0.2$, 0.5, 1, and 2 for the particle hardness. In addition, we explore particles softness values given by $\tau/\sigma_0 = 0.2$ (super soft), 0.1, 0.05 and 0.02 (super stiff). The corresponding free energy barriers are $1k_BT$, $6.1k_BT$, $26.7k_BT$ and $170k_BT$, respectively. In addition, the particle density, ρ_0, is also varied to study the role of compression of the size distribution and RDFs in bulk.

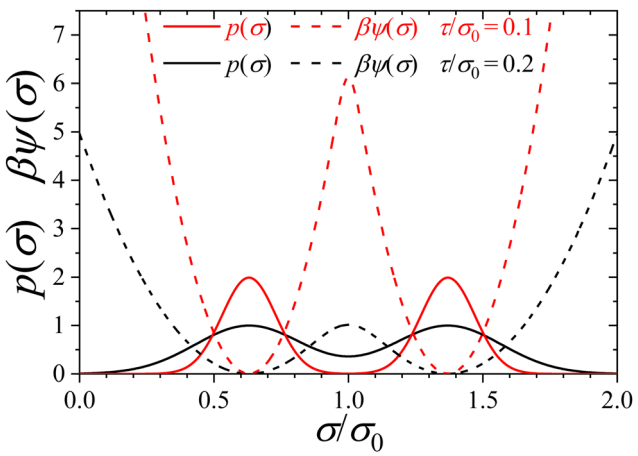

Fig. 1 Parent distribution of size, $p(\sigma)$, and its corresponding free-energy landscape, $\psi(\sigma)$, for two values of the particle softness: $\tau/\sigma_0 = 0.1$ (red lines) and $\tau/\sigma_0 = 0.2$ (black lines). In both cases, $\sigma_1 = 0.63\sigma_0$ and $\sigma_2 = 1.37\sigma_0$.

4 Perturbation theory

To complement the numerical DFT results with approximate analytical equations and limiting universal scaling laws, we perform a perturbation theory. For this, we use the isolated RC as basis and disturb it with a non-zero density ρ_0.[24] The mean force of a particle with size σ from particle–particle pair interactions is

$$K(\sigma) = -\rho_0\int\mathrm{d}\sigma' f(\sigma')\int\mathrm{d}\mathbf{r}\frac{\partial u(\mathbf{r};\sigma,\sigma')}{\partial\sigma}g(\mathbf{r};\sigma,\sigma'), \quad (29)$$

where the pair distribution function gives the probability for a certain configuration of two particles and $\partial u/\partial\sigma$ being the corresponding force for this configuration. In a next step we employ the mean-field approximation, $g(\mathbf{r};\sigma,\sigma') \approx 1$. By assuming

that the interaction potential u can be written as a function of $z = 2|\mathbf{r} - \mathbf{r}'|/(\sigma + \sigma')$, we obtain by substitution

$$K(\sigma) = -\rho_0\left(\int \mathrm{d}\sigma' f(\sigma')(\sigma+\sigma')^2\right)\underbrace{\left(-\frac{\pi}{2}\int_0^\infty \mathrm{d}z z^3 \frac{\partial u(z)}{\partial z}\right)}_{\equiv\kappa} = -\rho_0\kappa\int \mathrm{d}\sigma' f(\sigma')(\sigma+\sigma')^2 \quad (30)$$

with κ being an interaction potential coefficient. Consequently, this perturbation theory is universal for every interaction potential $u(z) = u(2r/(\sigma + \sigma'))$ with the condition that κ is finite. Because we find only a $\rho_0\kappa$-dependency, a different interaction potential (strength) just rescales with density. In our case of a Gaussian potential it holds $\beta\kappa = 0.375\pi^{3/2}\varepsilon$.

Eqn (30) can be written as expectation values of the emergent distribution

$$K(\sigma) = -\rho_0\kappa(\sigma^2 + 2\langle\sigma\rangle\sigma + \langle\sigma^2\rangle). \quad (31)$$

An integration leads to the free energy term from the interactions

$$F(\sigma) = -\int^\sigma \mathrm{d}\sigma' K(\sigma') = \frac{\rho_0\kappa}{3}(\sigma^3 + 3\langle\sigma\rangle\sigma^2 + 3\langle\sigma^2\rangle\sigma). \quad (32)$$

The total free energy $\psi_{\mathrm{tot}}(\sigma) = \psi(\sigma) + F(\sigma)$ is the sum of the bimodal single-particle potential $\psi(\sigma)$ and the perturbation $F(\sigma)$ which leads to the emergent distribution

$$f_{\mathrm{tot}}(\sigma) = f_0 \mathrm{e}^{-\beta\psi_{\mathrm{tot}}(\sigma)} = f_0 \mathrm{e}^{-\beta\psi(\sigma)}\mathrm{e}^{-\beta F(\sigma)} = f_0 p(\sigma)\mathrm{e}^{-\beta F(\sigma)}. \quad (33)$$

where $p(\sigma)$ is again the parent distribution consisting of two Gaussian distributions. The cubic term in eqn (32) hinders us to continue the analytical calculation. This is why we make a second order Taylor expansion of this term around σ_0 which is $\sigma^3 \approx 3\sigma_0\sigma^2 - 3{\sigma_0}^2\sigma +$ const. In addition, we use in eqn (32) the expectation values of the parent distribution $\langle\sigma\rangle = \sigma_0$ and $\langle\sigma^2\rangle = \tau^2 + ({\sigma_1}^2 + {\sigma_2}^2)/2$, which leads to

$$F(\sigma) = \rho_0\kappa\left(2\sigma_0\sigma^2 + \sigma\left(\tau^2 - \sigma_0^2 + \frac{{\sigma_1}^2 + {\sigma_2}^2}{2}\right)\right). \quad (34)$$

Consequently, eqn (33) is a multiplication and sum of different Gaussians. Therefore, $f_{\mathrm{tot}}(\sigma)$ can be calculated analytically with the technique of 'completing the square'. The calculation is shown in Appendix A and results in

$$f_{\mathrm{tot}}(\sigma) = A_0\left(B_1\exp\left[-\frac{(\sigma-\tilde{\sigma}_1)^2}{2\tilde{\tau}^2}\right] + B_2\exp\left[-\frac{(\sigma-\tilde{\sigma}_2)^2}{2\tilde{\tau}^2}\right]\right)$$

$$\text{with}\quad \tilde{\sigma}_i = \tilde{\tau}^2\left(\frac{\sigma_i}{\tau^2} - \beta\kappa\rho_0\left(\tau^2 - \sigma_0^2 + \frac{{\sigma_1}^2 + {\sigma_2}^2}{2}\right)\right),$$

$$\tilde{\tau}^2 = \frac{\tau^2}{1 + 4\beta\sigma_0\tau^2\rho_0\kappa}, \qquad B_i = \exp\left[\frac{\tilde{\sigma}_i^2}{2\tilde{\tau}^2} - \frac{\sigma_i^2}{2\tau^2}\right], \quad (35)$$

which is again the sum of two Gaussians, but with a new width $\tilde{\tau}$ and each with a new center $\tilde{\sigma}_i$ and weight B_i. The prefactor A_0 is just for normalization and is explicitly given in Appendix A. For the mean size we finally obtain

$$\langle\sigma\rangle = \frac{B_1\tilde{\sigma}_1 + B_2\tilde{\sigma}_2}{B_1 + B_2}. \quad (36)$$

5 Results and discussion

5.1 Compression effects on internal distributions and size

For a homogeneous bulk suspension without we need to solve eqn (20). Using the Gaussian pair potential (eqn (28)) and performing analytically the integral leads to the following expression for $f(\sigma)$ (see Appendix B):

$$f(\sigma) = q_0 p(\sigma)\exp\left(-\frac{\pi^{3/2}}{8}\varepsilon\rho_0\int_0^\infty \mathrm{d}\sigma'(\sigma+\sigma')^3 f(\sigma')\right), \quad (37)$$

being $q_0 \equiv q/\rho_0$ a normalization constant. Another choice for $u(r;\sigma,\sigma')$ such as the Hertzian pair potential leads to a similar expression for $f(\sigma)$, but with a different numerical prefactor. Consequently, the theoretical predictions presented below can be easily generalized to other functional dependencies of $u(r;\sigma,\sigma')$ by simply rescaling the particle density.

Fig. 2 shows the resulting size distributions for different particle densities from $\rho_0^* \equiv \rho_0\sigma_0^3 = 0$ to 5, for $\varepsilon = 2$. Each plot (from (a) to (d)) depicts the distributions for increasing particle stiffness. We first analyze the case of a soft RC, $\tau/\sigma_0 = 0.2$ (Fig. 2(a)). As observed, increasing ρ_0 modifies the bimodal distribution in such a way that small sizes occur with a larger probability than the big ones. For sufficiently large concentrations such as $\rho_0^* = 1.0$, the peak originally located at $\sigma_2 = 1.37\sigma_0$ (large sizes) has completely disappeared due to compression, and only small particles remain. In other words, crowding promotes the deswollen state due to the volume exclusion exerted by the soft RCs. This behavior has been reported in many bistable macromolecules such as flexible polymer chains, DNA and globular proteins.[5,7,20,32,41,52]

In addition to this particle redistribution, compression also provokes the shift of both peaks to smaller σ values. This effect is clearly seen for $\rho_0^* > 1.0$, for which the peak located initially at $\sigma_1 = 0.63\sigma_0$ experiences a notable increase and shifts to smaller sizes upon compression of the system. By increasing the particle stiffness (Fig. 2(b)–(d)) we still observe the size redistribution effect that converts big RC into small ones. However, the shifting to smaller sizes diminishes and becomes negligible in the limit of very stiff particles ($\tau/\sigma_0 = 0.02$), which means that it is extremely difficult to compress the volume of the RCs. This effect arises because the form of $\psi(\sigma)$ becomes very steep upon decreasing τ, so the energy cost of compressing the soft colloids tends to be large, too.

Fig. 3(a) depicts the average particle diameter of the RC fluid $(\langle\sigma\rangle = \int\sigma f(\sigma)\mathrm{d}\sigma)$ as a function of the bulk concentration, ρ_0, for different values of the repulsion strength, ε, assuming soft RCs with $\tau/\sigma_0 = 0.2$. For dilute systems and large mean pair distances, the compression effects are negligible, leading to

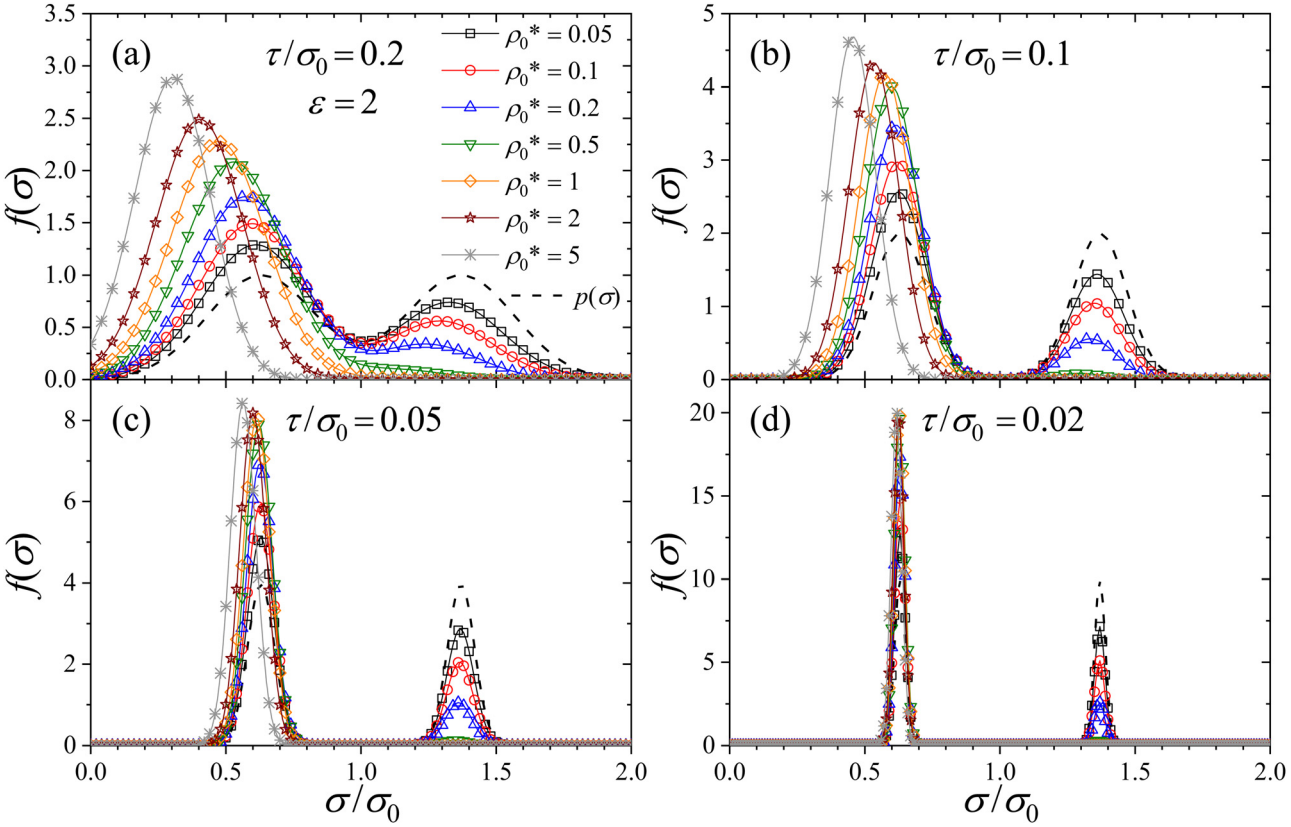

Fig. 2 Probability distributions of particle size for ε = 2 and $\rho_0^* = \rho_0\sigma_0^3$ = 0.05, 0.1, 0.2, 0.5, 1, 2 and 5. Plots from (a) to (d) show the distributions for increasing the particle stiffness: (a) τ/σ_0 = 0.2, (b) τ/σ_0 = 0.1, (c) τ/σ_0 = 0.05 and (d) τ/σ_0 = 0.02. The single-particle property distribution, $p(\sigma)$, is plotted as a reference (dashed lines).

$\langle\sigma\rangle\sigma_0 \approx 1$. However, by increasing ρ_0, the interparticle repulsion provokes a significant decrease of the mean size for larger values of ε.

By plotting $\langle\sigma\rangle$ against the coupling parameter $\rho_0\varepsilon$, we find that the different curves collapse onto a universal scaling curve (see orange line in the inset of Fig. 3(a)). This scaling behavior arises from the fact that the equilibrium distribution of a mean-field fluid, given by eqn (37), depends on the product $\varepsilon\rho_0$, so increasing the interparticle interaction strength, ε, at fixed ρ_0 has exactly the same effect on the probability distribution of sizes than increasing ρ_0 at fixed ε. At very large particle crowding, this scaling curve finally tends to follow an asymptotic power law decay, given by $\langle\sigma\rangle/\sigma_0 \sim (\rho_0^*\varepsilon)^{-0.4}$. Please note that similar results for the mean size and the size distribution will be obtained for any other non-Gaussian interparticle pair potential because of the rescalability of the potential dependent prefactor with the density ρ_0. The effect of the particle stiffness on $\langle\sigma\rangle$ is displayed in Fig. 3(b). We first describe the results for the bimodal $p(\sigma)$, given by eqn (26) (lines with symbols in Fig. 3(b)). It occurs that the mean size decreases in two stages due to two different processes: in the dilute regime conversion of big colloids into small ones takes place, whereas in the dense regime $(\rho_0^*\varepsilon > 1)$ particle compression dominates. For smaller values of τ both mechanisms become more and more separated. In other words, the big-to-small switching still occurs in the dilute regime, but the particle deswelling in the small state requires a further increase of the particle density due to particle stiffness. For sufficiently large densities, the scaling $\langle\sigma\rangle/\sigma_0 \sim (\rho_0^*\varepsilon)^{-0.4}$ is recovered, but larger compression is required to reach it (see for instance the curve for τ/σ_0 = 0.1). In the limit of very small τ (such as τ/σ_0 = 0.02), the particles are so stiff that they are not able to further reduce their volume under compression and we find a plateau located at $\langle\sigma\rangle \approx \sigma_1 = 0.63\sigma_0$. We point out that, although microgels cannot be modeled as ultrasoft Gaussian colloids, very similar behavior has also been reported in simulations of soft hollow microgels, which clearly show that deswelling of the particles under compression also follows two stages, with an intermediate region nearly having a plateau.[53] Note that within the validity of the mean-field approximation, other soft but non-Gaussian interaction potentials would lead to the same scaling behavior with ρ_0^*.

We remark here that the phase diagram of non-responsive repulsive Gaussian colloids shows crystallization and a reentrant fluid phase at high densities, but only for interaction strengths above $\varepsilon > 100$.[54,55] However, the values of ε explored in our work are well below this threshold. In addition, we believe that size responsiveness will promote even more the fluid phase due to the inherent size polydispersity of the system. Therefore, we do not expect the formation of solid phases, no matter the particle density.

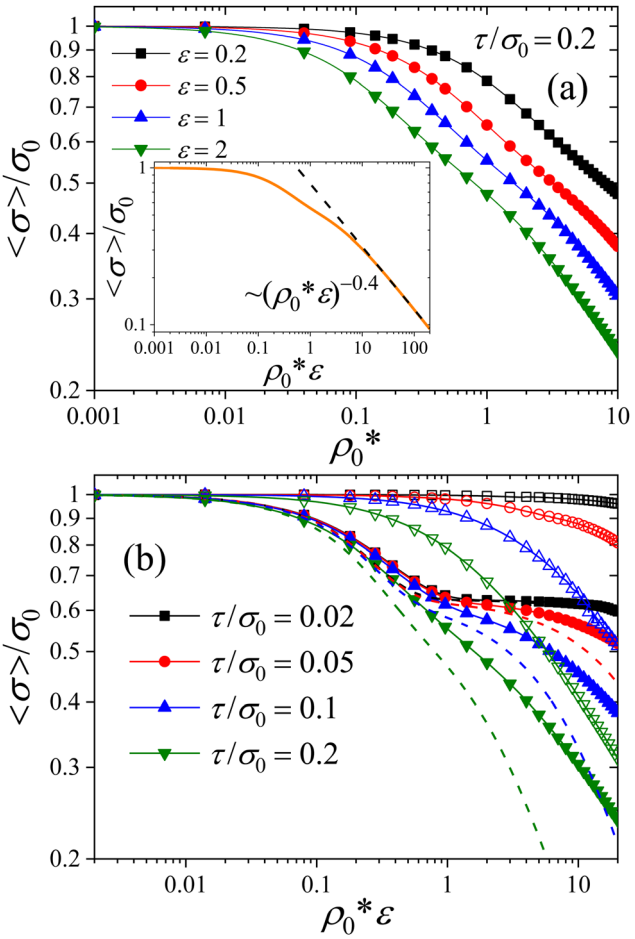

Fig. 3 (a) Average particle diameter, $\langle\sigma\rangle$, as a function of the particle concentration, ρ_0^*, for ε = 0.2, 0.5, 1 and 2. Inset: All curves for different ε collapse into a single curve when $\langle\sigma\rangle$ is plotted against $\rho_0^*\varepsilon$. For large particle densities, $\langle\sigma\rangle \sim (\rho_0^*\varepsilon)^{-1/3}$. (b) $\langle\sigma\rangle$ as a function of $\rho_0^*\varepsilon$ for different values of the particle softness: τ/σ_0 = 0.02, 0.05, 0.1 and 0.2. Lines with solid symbols correspond to the bimodal distribution (eqn (26)). Lines with open symbols show the results for the unimodal Gaussian distribution (eqn (27)). Dashed lines depict the predictions provided by the analytical perturbation theory (eqn (35) and (36)).

These results for the bimodal RCs can be compared to the ones obtained for an unimodal Gaussian distribution (lines with open symbols in Fig. 3(b)). In this case, the responsive colloids are not able to adapt to the density increase by converting big particles into small ones: the only possible mechanism is to reduce the particle size by uniform compression. As a consequence of this, the curves only show a single decay mode with $\rho_0^*\varepsilon$, also exhibiting the same scaling behavior for large compression of soft RCs. For the stiffer system (τ/σ_0 = 0.02), the reduction of the particle volume is almost negligible, so the particles behaves effectively as uncompressible non-responsive colloids.

We complement this discussion comparing the results for the mean size obtained with our mean-field responsive DFT with the theoretical predictions attained by the analytical perturbation theory (eqn (35) and (36) in Section 4), shown as dashed lines in Fig. 3(b) for different stiffnesses as a function of $\rho_0^*\varepsilon$. For small τ we find two decreases of $\langle\sigma\rangle$ that are separated by a plateau. Again, the interpretation is the same: the first one characterizes the transition of large particles into the small state, whereas the second decrease comes from the shrinking of the small state particles. As observed, although perturbation theory (involving low-density and mean-field approximation) is not able to exactly match the DFT predictions nor the right scaling trend for large $\rho_0^*\varepsilon$, at least it provides an excellent qualitative justification of the results in terms of an analytical expression.

5.2 Polydispersity

Another interesting property to investigate is the polydispersity of the size distribution, δ, defined as the ratio between the standard deviation and the mean size, *i.e.* $\delta = \sqrt{\langle\Delta\sigma\rangle^2}\Big/\langle\sigma\rangle \equiv \sqrt{\langle\sigma^2\rangle - \langle\sigma\rangle^2}\Big/\langle\sigma\rangle$. For the sake of simplicity, we start analysing the behavior of the RC with the Gaussian parent distribution (lines with open symbols in Fig. 4). As seen before, increasing ρ_0^* (or increasing ε) involves a progressive decrease of the particle mean size, especially for the softer colloids. Compression of the particles also entails a reduction of the absolute value of the standard deviation, $\sqrt{\langle\Delta\sigma\rangle^2}$, as expected (not shown). However, the polydispersity δ increases upon particle compression due to the reduction of the mean size. This effect is insignificant for the stiff systems (τ/σ_0 = 0.02 and 0.05), but becomes quite relevant for the softer system τ/σ_0 = 0.2, for which a significant increase of δ arises for $\rho_0^*\varepsilon > 1$. In other words, increasing the particle concentration leads to more polydisperse systems. This curious effect has been observed also in BD simulations of RCs interacting with an elastic Hertzian pair potential[24] as well as in experiments of soft microgel compression.[56]

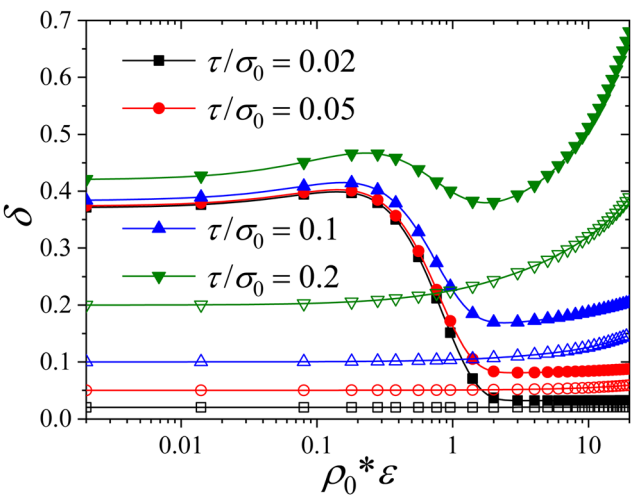

Fig. 4 RC polydispersity, $\delta = \langle\Delta\sigma^2\rangle^{1/2}/\langle\sigma\rangle$, as a function of $\rho_0^*\varepsilon$ for different values of the particle softness: τ/σ_0 = 0.02, 0.05, 0.1 and 0.2. Lines with solid symbols corresponding to the bimodal distribution (eqn (26)) and lines with open symbols to the unimodal Gaussian distribution (eqn (27)).

The behavior of the polydispersity δ for the bimodal RC system is more complex because of the two involved mechanisms (switching and compression) for the bistable particles. The corresponding curves are depicted as lines with solid symbols in Fig. 4. We first focus on the stiffer system, $\tau/\sigma_0 = 0.02$. For small particle densities (or weak interparticle interaction), in the regime $\rho_0^*\varepsilon < 0.2$, the reduction of the mean size due to the big-to-small conversion mechanism induces a slight increase of the polydispersity. For $0.2 < \rho_0^*\varepsilon < 1$ the bimodal distribution becomes completely unimodal, with a mean size located at $\sigma_1 = 0.63\sigma_0$, which obviously entails a substantial decrease of the polydispersity. In the regime $\rho_0^*\varepsilon > 1$, the polydispersity remains constant because the colloids are too stiff. This last regime is different for the softer colloids, for which the unimodal distribution obtained from switching from big to small sizes is still able to shift leftwards due to particle compression, giving rise to an increase of δ. This effect is clearly seen for $\tau/\sigma_0 = 0.2$, where a very important growth is observed for $\rho_0^*\varepsilon > 2$.

5.3 Packing fraction behavior

Particle compressibility can also be characterized by means of the particle volume fraction, defined from the emergent mean particle volume through

$$\phi = \frac{\pi}{6}\rho_0 \int f(\sigma)\sigma^3 \mathrm{d}\sigma. \tag{38}$$

Alternatively, we can also use the so-called generalized volume fraction, ζ, defined as the volume fraction of the soft particles assuming that they do not interact with each other (having the isolated particle distribution $p(\sigma)$),[25,57–59]

$$\zeta = \frac{\pi}{6}\rho_0 \int p(\sigma)\sigma^3 \mathrm{d}\sigma. \tag{39}$$

It is important to emphasize that the definition of the packing fraction given in eqn (38) does not take into account the mutual volume overlap or shape deformation of the soft colloids upon compression, which cannot be accessed by means of this theoretical framework. Therefore, eqn (38) represents only a possible reasonable definition for ϕ that provides an estimate of how particle squeezing depends on the density and the softness for interacting systems.

Fig. 5(a) illustrates $\phi(\zeta)$ for our bistable RCs with $\tau/\sigma_0 = 0.2$. At high dilution, particle interactions are so weak that particle compression is practically negligible, leading to $\phi = \zeta$. Increasing the particle concentration, the compression of the soft colloids leads to $\phi < \zeta$. Please note that ζ can rise well above 1, which means that our RCs are able to significantly modify their volume in presence of crowding or other external interactions. This reduction in the particle volume becomes emphasized as we increase the interparticle repulsion strength. Indeed, for $\varepsilon = 0.2$ particle squeezing starts to become relevant above $\zeta > 0.3$, whereas for $\varepsilon = 2$ particle compression is important already for $\zeta > 0.1$, and becomes even more significant for larger ζ. In fact, soft colloids become about 15 times smaller in volume for $\zeta = 1.5$ due to particle interactions for $\varepsilon = 2$.

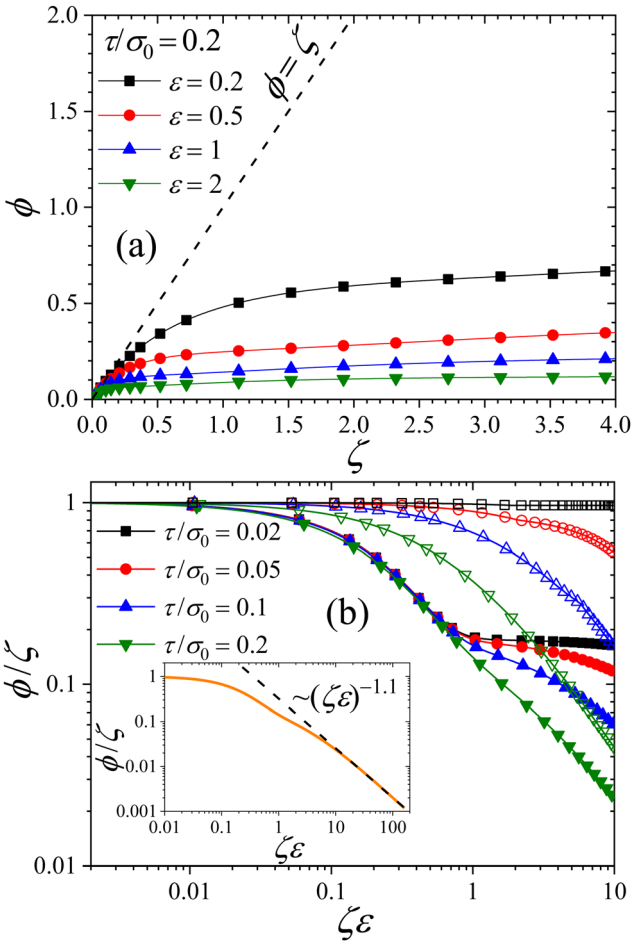

Fig. 5 (a) Particle volume fraction (ϕ) as a function of the generalized volume fraction (ζ) for $\tau/\sigma = 0.2$, and for different values of the repulsion strength: $\varepsilon = 0.2$, 0.5, 1 and 2. (b) ϕ/ζ as a function of $\zeta\varepsilon$ for different values of the particle softness: $\tau/\sigma_0 = 0.02$, 0.05, 0.1 and 0.2. Inset: All curves obtained for $\tau/\sigma_0 = 0.2$ for different values of ε collapse into a common form when ϕ/ζ is plotted against $\zeta\varepsilon$. For large particle densities, $\phi/\zeta \sim (\zeta\varepsilon)^{-1.1}$.

The behavior of the ratio ϕ/ζ as a function of $\zeta\varepsilon$ for a fixed stiffness is plotted in Fig. 5(b) for different values of τ (solid symbols correspond to the bimodal distribution and open symbols to the unimodal one). As observed, the curves for the bimodal parent distribution (eqn (26)) follow the same trends than the ones discussed for $\langle\sigma\rangle$: for $\zeta\varepsilon < 0.7$ (dilute or weakly interacting colloids), the particle volume diminishes due to conversion of big colloids into small ones, whereas for large enough $\zeta\varepsilon$ the decrease in particle volume is caused by the continuous shrinking of the particles. Again, the curves scale into a common form due to the mean-field character of our RC fluid. This is clearly seen in the inset of Fig. 5(b), in which the orange line represents the curves obtained for different values of ε. For large particle densities, the scaling finally tends to follow a power law decay given by $\phi/\zeta \sim (\zeta\varepsilon)^{-1.1}$.

The results for the unimodal Gaussian parent distribution (eqn (27)) do not show the big-to-small transition, as expected. In this case, the curves have two well-defined regimes: in the low-density regime $\zeta\varepsilon < 0.3$–0.4 the responsive colloids do not reduce their internal volume. This regime corresponds to a mutual interpenetration due to the overlap of the particles, without particle compression. For larger concentrations, the interpenetration regime saturates, and the only mechanism able to accommodate the RCs is reducing their particle volume, being more significant for softer colloids.

5.4 Osmotic pressure

In the mean-field approximation, the bulk pressure of a homogeneous multi-component colloidal system with M particle species of different sizes σ_i and with a total number density ρ_0 is

$$P_{\text{bulk}} = \rho_0 k_B T + \frac{1}{2}\rho_0^2 \sum_{i=1}^{M}\sum_{j=1}^{M} x_i x_j \int u(r;\sigma_i,\sigma_j)\mathrm{d}\mathbf{r}, \qquad (40)$$

where x_i represents the fraction of particles of size σ_i, and $u(r,\sigma_i,\sigma_j)$ is the pair interaction potential between two particles of sizes σ_i and σ_j separated by a distance r. This expression can be generalized for the mean-field RC fluid as

$$P_{\text{bulk}} = \rho_0 k_B T + \frac{1}{2}\rho_0^2 \int \mathrm{d}\sigma \int \mathrm{d}\sigma' f(\sigma) f(\sigma') \int u(r;\sigma,\sigma')\mathrm{d}\mathbf{r}, \qquad (41)$$

Inserting the Gaussian pair potential given by eqn (28) leads to the following expression for the bulk pressure,

$$P_{\text{bulk}} = \rho_0 k_B T + \frac{\pi^{3/2}}{16}\rho_0^2 \varepsilon \int \mathrm{d}\sigma \int \mathrm{d}\sigma' f(\sigma) f(\sigma')(\sigma+\sigma')^3 \qquad (42)$$

Fig. 6(a) shows the bulk pressure as a function of the particle density for a bimodal distribution of particles (eqn (26)) with $\tau/\sigma_0 = 0.2$ (soft colloids), for four different values of the interaction strength, going from $\varepsilon = 0.2$ to 2. As expected, P_{bulk} increases with ρ_0. In principle, one would expect to find an increase of P_{bulk} also with the interparticle repulsion (that is, the particle hardness), ε. In fact, this would be the case for an ordinary non-responsive system of colloids. However, we find here a surprising observation: the equilibrium pressure is rather insensitive to ε in the range of studied particle densities. This result implies that, when particle hardness is enhanced, the RC fluid modifies the size distribution by conversion/squeezing to smaller sizes in order to reduce the interparticle repulsion, leading to a the pressure that remains almost unaltered. Such a homeostatic effect is a characteristic feature of responsive colloids and can also be observed *e.g.*, for self-diffusion.[24]

In Fig. 6(b) we plot the dependence of the bulk pressure on density and varying the particle softness. As observed, decreasing particle softness does not modify P_{bulk} for $\rho_0^* < 0.8$, because in this dilute regime the compression of the systems leads to a rearrangement of the bimodal distribution in such a way that the population of the big colloids decreases whereas the population of the small ones increases. This redistribution of

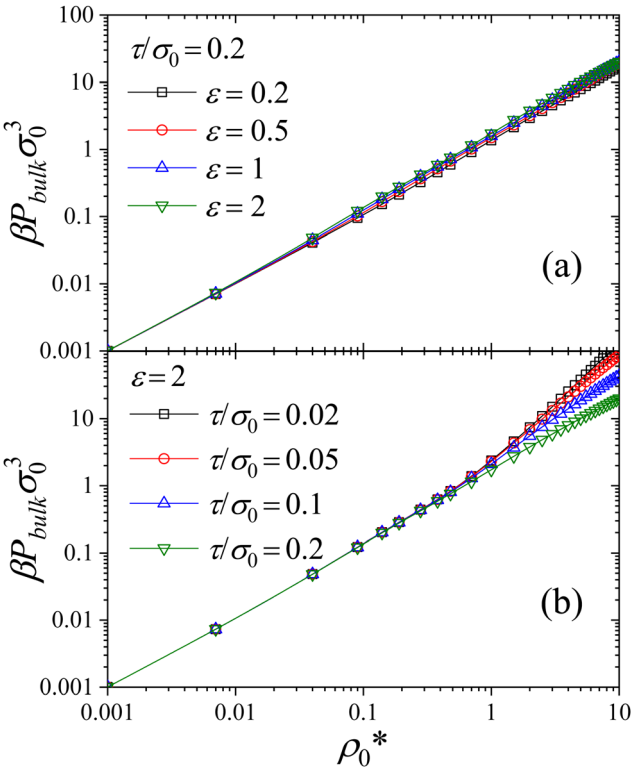

Fig. 6 (a) Bulk pressure of the RC fluid as a function of the particle concentration for different values of the interparticle repulsion strength, ε = 0.2, 0.5, 1 and 2. In all cases τ/σ_0 = 0.2. (b) Bulk pressure as a function of the particle concentration for different values of the particle softness, τ/σ_0 = 0.02, 0.05, 0.1 and 0.2. In all cases ε = 2.

sizes occurs independently of the particle stiffness, leading to the same pressure of the system in all cases. The situation changes when $\rho_0^* > 0.8$. In this regime, big colloids have already disappeared in the system, so increasing the particle concentration only provokes the progressive compression of the small colloids. Since squeezing stiff colloids involves an additional energy cost compared to soft ones, we find that the bulk pressure becomes dependent on the particle stiffness, with larger P_{bulk} for smaller τ.

5.5 Radial distribution functions (RDFs)

The RDFs are obtained solving iteratively eqn (23) and then using eqn (24). The calculation of $\mu_{\text{ex}}(r,\sigma)$ for the particular case of a Gaussian pair potential is shown in Appendix C (see eqn (57)).

Fig. 7(a)–(c) shows the resulting $g(r;\sigma,\sigma')$ of a uniform RC fluid for τ/σ_0 = 0.2 and for several combinations of σ and σ', *i.e.* small–small (σ_1-σ_1), big–small (σ_1-σ_2), and big–big (σ_2-σ_2). The RDFs usually feature an excluded-volume 'correlation' hole at small distances that grows with the size of both particles. This depletion region is the consequence of the existent soft repulsive particle–particle interactions.[37] In the regime of low particle concentration $(\rho_0^* \ll 1)$, the DFT results clearly show that the equilibrium RDF tends to $\lim_{\rho_0\to 0} g(r;\sigma,\sigma') = \exp(-\beta u(r;\sigma,\sigma'))$, as expected. Increasing ρ_0 yields a progressive

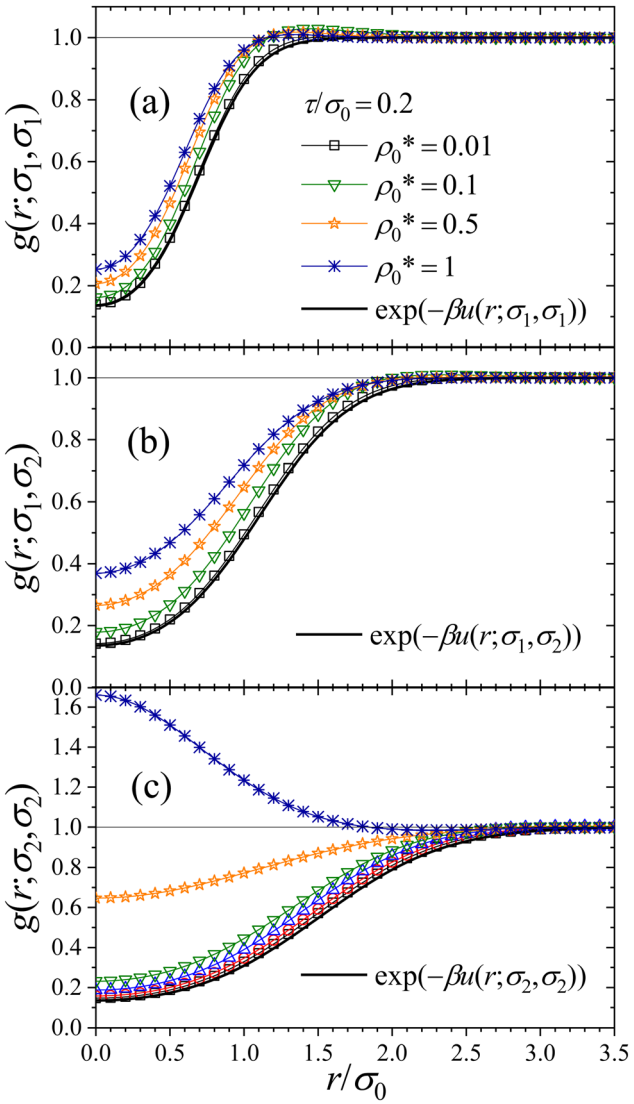

Fig. 7 Radial distribution functions (RDFs), $g(r;\sigma,\sigma')$ as a function of the interparticle distance, r, for different values of the particle concentration, and for different combinations of the sizes: (a) $g(r,\sigma_1,\sigma_1)$, (b) $g(r,\sigma_1,\sigma_2)$ and (c) $g(r,\sigma_2,\sigma_2)$, where $\sigma_1 = 0.63\sigma_0$ and $\sigma_2 = 1.37\sigma_0$. Black solid lines represent the low density limit, $g(r,\sigma,\sigma') \approx \exp(-\beta u(r,\sigma,\sigma'))$. In all cases, $\varepsilon = 2$ and $\tau/\sigma_0 = 0.2$.

reduction of the soft correlation hole. This is a typical behavior of finite core interacting colloids, which tend to overlap under compression, leading to an ideal-gas-like behavior of $g(r)$ in the high density limit.[37,49] Surprisingly, the RDF between two big colloids develops a maximum at $r = 0$ upon increasing the particle concentration (see blue curve in Fig. 7(c)), indicating the existence of a depletion attraction between them. Indeed, for $\rho_0^* = 1$ the big colloids are scarce in the system. So, when two big RC approach each other, small particles are excluded from the region between the big particles, inducing a depletion interaction given by $\beta u_{\mathrm{depl}}(r) = -\ln g(r;\sigma_2,\sigma_2)$.

It is important to emphasize that the size distribution of the homogeneous RC fluid is position-dependent with respect to a fixed test particle. In other words, the distribution changes locally when we examine it close to one particle or far away from it. This effect is visible in Fig. 8, where the position-dependent size distribution ($f(\mathbf{r},\sigma)$) of the colloids surrounding a central big particle with size $\sigma_2 = 1.37\sigma_0$ is plotted for the particles located at $r = 0$ and at $r \to \infty$ (*i.e.* in bulk solution), for $\rho_0^* = 0.1$, $\varepsilon = 2$ and $\tau/\sigma_0 = 0.2$. The size distribution in bulk (red curve) is in accordance with the results shown before in Fig. 2(a). However, when approaching $r = 0$, the repulsion exerted by the central big colloid induces a decrease of the local density, as predicted by the depletion observed in $g(r;\sigma_1,\sigma_2)$. Since the concentration of particles is smaller in this region, the RC fluid becomes less squeezed, allowing the increase of population of big colloids, as seen in the black curve of Fig. 8.

Finally, we explore the role of the particle stiffness on the microstructure of the RC fluid. On the one hand, calculations performed for different values of τ show that the RDFs $g(r;\sigma,\sigma')$ are barely dependent on the particle stiffness for dilute systems $(\rho_0^* < 0.8)$. Somehow, it happens that the effect of the stiffness is compensated by the already discussed rearrangement of the bimodal size distribution, leaving the bulk properties as well as the pressure and the microstructure unaltered (results not shown). On the other hand, for $\rho_0^* > 0.8$, big colloids have almost disappeared from the system, and the only way to react under compression is by isotropic shrinking of the colloids. In this regime, the microstructure becomes sensitive to the particle stiffness, as seen in Fig. 9. Indeed, increasing stiffness makes the particle more repulsive, increasing the bulk pressure, and pushing the colloids closer, which leads to a reduction of the correlation hole of $g(r,\sigma_1,\sigma_1)$ and $g(r,\sigma_1,\sigma_2)$ (see Fig. 9(a) and (b)). As a consequence of the reduction of the depletion region of small colloids around the big ones, the maximum observed in $g(r;\sigma_2,\sigma_2)$ also decreases. This result implies that softer colloids are able to induce stronger depletion forces than stiff ones in RC fluids.

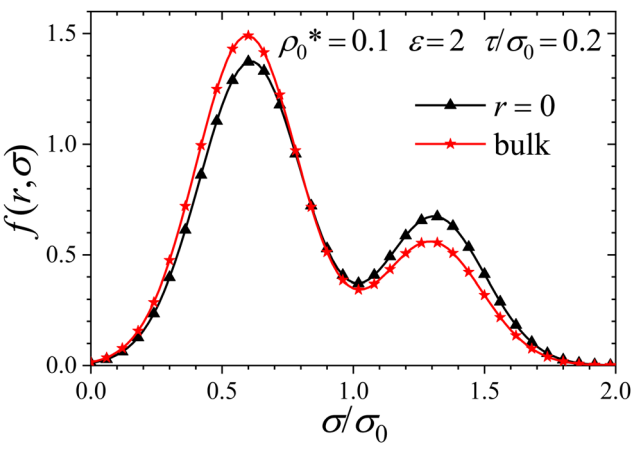

Fig. 8 Position-dependent size distribution of the RC fluid surrounding a central colloid of size $\sigma_2 = 1.37\sigma_0$, calculated for $\rho_0^* = 0.1$, $\varepsilon = 2$ and $\tau/\sigma_0 = 0.2$. Black line shows the size distribution at $r = 0$, whereas the red curve represents the distribution far away from the central colloid (bulk).

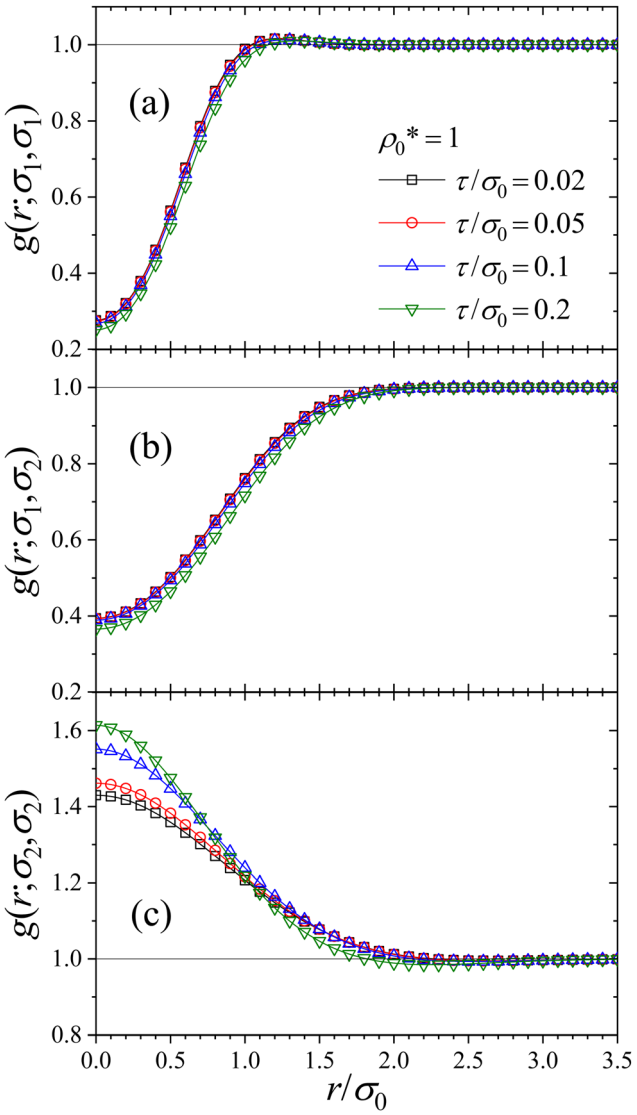

Fig. 9 RDFs, $g(r;\sigma,\sigma')$ as a function of the interparticle distance, r, for different values of the particle softness, and for different combinations of particle sizes: (a) $g(r,\sigma_1,\sigma_1)$, (b) $g(r,\sigma_1,\sigma_2)$ and (c) $g(r,\sigma_2,\sigma_2)$, where $\sigma_1 = 0.63\sigma_0$ and $\sigma_2 = 1.37\sigma_0$. In all cases $\varepsilon = 2$ and $\rho_0^* = 0.1$.

6 Conclusions

In this work, we applied a mean-field DFT to characterize the structural properties of a homogeneous fluid comprised by soft (Gaussian) responsive colloids in which the particle size (σ) is explicitly responsive and bistable. This fundamental model represents a first approach to describe macromolecular crowding effects in soft two-state biomolecules and polymer-based systems, which are able to modify the particle internal conformation in response to changes in the particle concentration and particle–particle interactions. The results show that compressing the system shifts the bimodal free-energy landscape to promote smaller sizes following a two-stage transition that can be tuned by varying the particle softness. In the first stage, for low particle densities, compression of the system shifts big colloids into small ones. In the second stage, at high particle densities, compression induces a progressive reduction of the size of the small colloids. The separation between these two compression regimes is enhanced by increasing the stiffness of the individual particles. This behavior represents a new feature that is not observed in simpler unimodal landscapes. In addition, particle–particle interactions significantly lower volume fractions compared to the ones observed in noninteracting systems. More precisely, we find for both the mean size and the particle volume fraction follow a scaling law in the regime of high densities with particle concentration (ρ_0) and interaction strength (ε) as basis. Furthermore, a study of the osmotic pressure demonstrates that the bulk pressure is almost independent of the interaction strength. This surprising effect is attributed to the responsiveness of the soft particles. Finally, we show that mean-field DFT with the Test Particle Route also provides micro-structural information of the fluid of responsive colloids, through the radial pair–property distribution, $g(r;\sigma,\sigma')$. Here, for increased densities the remaining large particles possess an effective attraction to each other due to depletion effects.

Overall, by comparing unimodal to bimodal size distributions in our model systems we uncover typical signatures of bistability in the compression behavior. For example, saddle-point like behavior in the mean size or packing fraction *versus* density, or intriguing non-monotonicities in the particle polydispersity.

Our model could also serve as a very preliminary description of the physics behind microgel volume transitions arising close to the LCST.[60–62] In fact, experiments performed with a single thermo-responsive microgel using optical tweezers clearly show that the transition from the swollen to the collapsed state is discontinuous, suggesting that this process represents a first-order phase transition, and thus leading to a distinct two-state behavior and hysteresis.[63,64] In fact, hysteresis – as a marker for bistability – in swelling–deswelling cycles of (ionized and non-ionized) hydrogels were found induced by temperature,[65–67] pH,[22,66,68] or the addition of cosolutes.[69,70] However, it is important to emphasize that the application of our method to the description of microgels implies important changes of the model presented here. First, the Gaussian pair potential must be replaced by a more adequate interaction model, such as the Hertzian pair potential, and also include the size-dependence on the interaction strength, $\varepsilon(\sigma,\sigma')$, as suggested by Scotti *et al.*[53] Second, the mean-field approach described in the work should be improved using a more accurate DFT to account for the harder character of the particle interactions arising by the presence of crosslinker inside the microgel particle. Finally, experiments and simulations with squeezed microgel systems indicate the existence of a deformation regime (faceting) that appears between the interpenetration and the compression regimes, in which the individual particles change their shapes without reducing their volume.[71–77] To account for faceting, additional internal coarse-grained parameters beyond σ should also be included in the model.

In the future we would like to investigate how RC fluids behave under different external potentials. The relevance of external potentials is given in both *in vitro* and *in vivo*. They can

exist either as an immutable present field (*e.g.*, gravitation) or a tuneable perturbation (*e.g.*, light) to obtain a control mechanism. Finally, we would like to study how the presence of internal DoF affects the phase behavior of RC fluids in the presence of interparticle attractions, for both unimodal and bimodal distribution. For the case of repulsion, it is well known that the phase diagram of non-responsive Gaussian colloids shows crystallization and a reentrant fluid phase at large enough densities for $\varepsilon > 100$.[54,55] Therefore, it would be very interesting to investigate how particle responsiveness modifies this phase behavior as a function of the particle softness, possibly enhancing the fluid phase and reducing the regions with solid phases. Extending our method to other repulsive ultrasoft repulsive potentials as the generalized exponential models (GEM-*n*) would also allow to explore the effect of responsiveness on the anomalous formation of microclusters arranged into crystal structures observed in this kind of systems.[38,78–81]

Conflicts of interest

There are no conflicts to declare.

Appendices

Appendix A: calculation of the emergent distribution in the perturbation theory

The goal of this calculation is to obtain the emergent distribution $f_{\mathrm{tot}}(\sigma)$ from the perturbation theory (eqn (33) and (34)). The last two equations read

$$f_{\mathrm{tot}}(\sigma) = f_0 p(\sigma) \mathrm{e}^{-\beta F(\sigma)}, \tag{43}$$

$$F(\sigma) = -\rho_0 \kappa \left(2\sigma_0 \sigma^2 + \sigma \left(\tau^2 - \sigma_0^2 + \frac{{\sigma_1}^2 + {\sigma_2}^2}{2} \right) \right), \tag{44}$$

where $p(\sigma)$ is the parent distribution of the form (see eqn (26))

$$p(\sigma) = \frac{1}{2\sqrt{2\pi\tau^2}} \left[\underbrace{\exp\left(-\frac{(\sigma - \sigma_1)^2}{2\tau^2} \right)}_{p_1(\sigma)} + \underbrace{\exp\left(-\frac{(\sigma - \sigma_2)^2}{2\tau^2} \right)}_{p_2(\sigma)} \right]. \tag{45}$$

Consequently, the emergent distribution can be written as

$$f_{\mathrm{tot}}(\sigma) = f_0 (p_1(\sigma) + p_2(\sigma)) \mathrm{e}^{-\beta F(\sigma)}. \tag{46}$$

with a normalization factor f_0. One of the two terms can be written as

$$\begin{aligned} p_1(\sigma)\mathrm{e}^{-\beta F(\sigma)} == \exp\Bigg[& -\frac{(\sigma - \sigma_1)^2}{2\tau^2} - 2\rho_0 \kappa \sigma_0 \sigma^2 \\ & -\rho_0 \kappa \sigma \left(\tau^2 - {\sigma_0}^2 + \frac{{\sigma_1}^2 + {\sigma_2}^2}{2\tau^2} \right) \Bigg] \end{aligned} \tag{47}$$

$$\begin{aligned} = \exp\Bigg[& -\frac{\sigma^2}{2} \underbrace{\left(\frac{1}{\tau^2} + 4\rho_0 \kappa \sigma_0 \right)}_{\equiv 1/\tilde{\tau}^2} \\ & + \sigma \left(\frac{2\sigma_1}{2\tau^2} - \rho_0 \kappa \left(\tau^2 - {\sigma_0}^2 + \frac{{\sigma_1}^2 + {\sigma_2}^2}{2\tau^2} \right) \right) - \frac{{\sigma_1}^2}{2\tau^2} \Bigg] \end{aligned} \tag{48}$$

$$= \exp\left[-\frac{\sigma^2}{2\tilde{\tau}^2} + \frac{2\sigma}{2\tilde{\tau}^2} \underbrace{\tilde{\tau}^2 \left(\frac{\sigma_1}{\tau^2} - \rho_0 \kappa \left(\tau^2 - {\sigma_0}^2 + \frac{{\sigma_1}^2 + {\sigma_2}^2}{2\tau^2} \right) \right)}_{\equiv \tilde{\sigma}_1} - \frac{\sigma_1^2}{2\tau^2} \right] \tag{49}$$

$$= \exp\left[-\frac{(\sigma - \tilde{\sigma}_1)^2}{2\tilde{\tau}^2} \right] \underbrace{\exp\left[\frac{\tilde{\sigma}_1^2}{2\tilde{\tau}^2} - \frac{{\sigma_1}^2}{2\tau^2} \right]}_{\equiv B_1}. \tag{50}$$

Therewith, we obtain with an analogous calculation for $p_2(\sigma)\mathrm{e}^{-\beta F(\sigma)}$ and a renormalization the solution for the emergent distribution

$$\begin{aligned} f_{\mathrm{tot}}(\sigma) = & \underbrace{\frac{1}{B_1 + B_2\sqrt{2\pi\tilde{\tau}^2}}}_{A_0} \Bigg(B_1 \exp\left[-\frac{(\sigma - \tilde{\sigma}_1)^2}{2\tilde{\tau}^2} \right] \\ & + B_2 \exp\left[-\frac{(\sigma - \tilde{\sigma}_2)^2}{2\tilde{\tau}^2} \right] \Bigg) \end{aligned} \tag{51}$$

which coincides again with eqn (35).

Appendix B: calculation of μ_{ex} for an homogeneous mean-field fluid

For a homogeneous RC fluid (no external fields), the particle density can be written as $\rho(r,\sigma) = \rho_0 f(\sigma)$, so it does not depend on r. Consequently, the double integral involved in the calculation of $\mu_{\mathrm{ex}}(r,\sigma)$ in the mean-field approximation can be simplified as

$$\begin{aligned} \mu_{\mathrm{ex}}(r,\sigma) &= \int \mathrm{d}\mathbf{r}' \int \mathrm{d}\sigma' \rho(\mathbf{r}', \sigma') u(\mathbf{r}, \mathbf{r}'; \sigma, \sigma') \\ &= \varepsilon \rho_0 \int \mathrm{d}\sigma' f(\sigma') \int \mathrm{d}\mathbf{r}' \mathrm{e}^{-4|\mathbf{r}-\mathbf{r}'|^2/(\sigma+\sigma')^2} \\ &= \varepsilon \rho_0 \int \mathrm{d}\sigma' f(\sigma') \int_0^\infty 4\pi r'^2 \mathrm{e}^{-4r'^2/(\sigma+\sigma')^2} \mathrm{d}r' \end{aligned} \tag{52}$$

Integration over the r' radial coordinate leads to an excess chemical potential that only depends on the particle size, σ:

$$\mu_{ex}(\mathbf{r},\sigma) = \mu_{ex}(\sigma) = \frac{\varepsilon\rho_0\pi^{3/2}}{8}\int_0^\infty d\sigma'(\sigma+\sigma')^3 f(\sigma'). \quad (53)$$

Appendix C: calculation of μ_{ex} for a RC fluid confined inside a spherical cavity

For spherical symmetry, the density profile depends on $\rho(\mathbf{r},\sigma) = \rho(r,\sigma)$, where r is the radial coordinate, or distance to the center of the cavity. In this case, the excess chemical potential of a mean-field fluid of Gaussian colloids is

$$\mathbf{r}'\mu_{ex}(r,\sigma) = \varepsilon\int d\mathbf{r}'\int d\sigma'\rho(r',\sigma')e^{-4|\mathbf{r}-\mathbf{r}'|^2/(\sigma+\sigma')^2}. \quad (54)$$

Without the lose of generality, We can chose r to be oriented in the z direction, $\mathbf{r} = r\hat{k}$, so

$$|\mathbf{r} - \mathbf{r}'|^2 = r^2 + r'^2 - 2rr'\cos\theta', \quad (55)$$

which leads to

$$\begin{aligned}\mu_{ex}(r,\sigma) &= \varepsilon\int d\sigma'\int_0^{2\pi} d\phi'\int_0^{\pi} d\theta'\int_0^R r'^2 dr'\sin\theta'\rho(r',\sigma') \\ &\times e^{-4r^2/(\sigma+\sigma')^2}e^{-4r'^2/(\sigma+\sigma')^2}e^{8rr'\cos\theta'/(\sigma+\sigma')^2},\end{aligned} \quad (56)$$

where R is the radius of the spherical compartment. Integrating over ϕ' and θ' provides the final expression for $\mu_{ex}(r,\sigma)$

$$\begin{aligned}\mu_{ex}(r,\sigma) &= \frac{\varepsilon\pi}{2r}\int d\sigma'(\sigma+\sigma')^2 e^{-4r^2/(\sigma+\sigma')^2} \\ &\times \int_0^R dr' r' e^{-4r'^2/(\sigma+\sigma')^2}\sinh\left(\frac{8rr'}{(\sigma+\sigma')^2}\right)\rho(r',\sigma')\end{aligned} \quad (57)$$

Acknowledgements

The authors thank M. A. Fernández-Rodríguez (University of Granada) for helpful discussions. A. M.-J. thanks the financial support provided by the Junta de Andalucía and European Regional Development Fund – *Consejería de Conocimiento, Investigación y Universidad, Junta de Andalucía* (Projects PY20-00241, A-FQM-90-UGR20) and the program Visiting Scholars funded by the *Plan Propio* of the University of Granada (Project PPVS2018-08).

References

1 S. B. Zimmerman and A. P. Minton, *Annu. Rev. Biophys. Biomol. Struct.*, 1993, **22**, 27–65.
2 R. Ellis, *Trends Biochem. Sci.*, 2001, **26**, 597–604.
3 H.-X. Zhou, G. Rivas and A. P. Minton, *Annu. Rev. Biophys.*, 2008, **37**, 375–397.
4 Y. C. Kim and J. Mittal, *Phys. Rev. Lett.*, 2013, **110**, 208102.
5 H. Kang, P. A. Pincus, C. Hyeon and D. Thirumalai, *Phys. Rev. Lett.*, 2015, **114**, 068303.
6 J. Shin, A. G. Cherstvy and R. Metzler, *Soft Matter*, 2015, **11**, 472–488.
7 M. P. Taylor, C. Vinci and R. Suzuki, *J. Chem. Phys.*, 2020, **153**, 174901.
8 A. P. Minton, *J. Biol. Chem.*, 2001, **276**, 10577–10580.
9 G. Rivas, J. A. Fernández and A. P. Minton, *Proc. Natl. Acad. Sci. U. S. A.*, 2001, **98**, 3150–3155.
10 S. L. Speer, C. J. Stewart, L. Sapir, D. Harries and G. J. Pielak, *Annu. Rev. Biophys.*, 2022, **51**, 267–300.
11 C. Tan, S. Saurabh, M. P. Bruchez, R. Schwartz and P. LeDuc, *Nat. Nanotechnol.*, 2013, **8**, 602–608.
12 K. P. Amiri, A. Kalish and S. Mukherji, *Phys. Rev. Lett.*, 2023, **130**, 018401.
13 S. D. Quinn, L. Dresser, S. Graham, D. Conteduca, J. Shepherd and M. C. Leake, *Front. Bioeng. Biotechnol.*, 2022, **10**, 958026.
14 K. W. Plaxco, K. T. Simons, I. Ruczinski and D. Baker, *Biochemistry*, 2000, **39**, 11177–11183.
15 X. Zeng, K. M. Ruff and R. V. Pappu, *Proc. Natl. Acad. Sci. U. S. A.*, 2022, **119**, e2200559119.
16 H. K. Murnen, A. R. Khokhlov, P. G. Khalatur, R. A. Segalman and R. N. Zuckermann, *Macromolecules*, 2012, **45**, 5229–5236.
17 U. B. Choi, J. J. McCann, K. R. Weninger and M. E. Bowen, *Structure*, 2011, **19**, 566–576.
18 S. Dhiman, A. Jain and S. J. George, *Angew. Chem., Int. Ed.*, 2017, **56**, 1329–1333.
19 N. F. Dupuis, E. D. Holmstrom and D. J. Nesbitt, *Proc. Natl. Acad. Sci. U. S. A.*, 2014, **111**, 8464–8469.
20 N. Tokuriki, M. Kinjo, S. Negi, M. Hoshino, Y. Goto, I. Urabe and T. Yomo, *Protein Sci.*, 2004, **13**, 125–133.
21 E. Sato Matsuo and T. Tanaka, *J. Chem. Phys.*, 1988, **89**, 1695–1703.
22 A. Suzuki and H. Suzuki, *J. Chem. Phys.*, 1995, **103**, 4706–4710.
23 Y.-C. Lin, B. Rotenberg and J. Dzubiella, *Phys. Rev. E*, 2020, **102**, 042602.
24 U. Baul and J. Dzubiella, *J. Phys.: Condens. Matter*, 2021, **33**, 174002.
25 M. Urich and A. R. Denton, *Soft Matter*, 2016, **12**, 9086–9094.
26 U. Baul, N. Götth, M. Bley and J. Dzubiella, *J. Chem. Phys.*, 2021, **155**, 244902.
27 M. Schmidt, *Rev. Mod. Phys.*, 2022, **94**, 015007.
28 J.-P. Hansen and I. McDonald, *Theory of Simple Liquids*, Academic Press, 4th edn, 2013.
29 J. L. Barrat and J. P. Hansen, *J. Phys.*, 1986, **47**, 1547–1553.
30 I. Pagonabarraga, M. E. Cates and G. J. Ackland, *Phys. Rev. Lett.*, 2000, **84**, 911–914.
31 A. R. Denton and M. Schmidt, *J. Phys.: Condens. Matter*, 2002, **14**, 12051–12062.
32 M. S. Cheung, D. Klimov and D. Thirumalai, *Proc. Natl. Acad. Sci. U. S. A.*, 2005, **102**, 4753–4758.
33 C. L. Vestergaard, P. C. Blainey and H. Flyvbjerg, *Nucleic Acids Res.*, 2018, **46**, 2446–2458.

34 J. Heyda, S. Soll, J. Yuan and J. Dzubiella, *Macromolecules*, 2014, **47**, 2096–2102.
35 P. G. Bolhuis, A. A. Louis, J. P. Hansen and E. J. Meijer, *J. Chem. Phys.*, 2001, **114**, 4296–4311.
36 A. A. Louis, P. G. Bolhuis, J. P. Hansen and E. J. Meijer, *Phys. Rev. Lett.*, 2000, **85**, 2522–2525.
37 A. A. Louis, P. G. Bolhuis and J. P. Hansen, *Phys. Rev. E: Stat. Phys., Plasmas, Fluids, Relat. Interdiscip. Top.*, 2000, **62**, 7961–7972.
38 C. N. Likos, N. Hoffmann, H. Löwen and A. A. Louis, *J. Phys.: Condens. Matter*, 2002, **14**, 7681.
39 J. K. Percus, *Phys. Rev. Lett.*, 1962, **8**, 462–463.
40 A. J. Archer, P. Hopkins and M. Schmidt, *Phys. Rev. E: Stat., Nonlinear, Soft Matter Phys.*, 2007, **75**, 040501.
41 E. Sherman and G. Haran, *Proc. Natl. Acad. Sci. U. S. A.*, 2006, **103**, 11539–11543.
42 I. C. Sanchez, *Macromolecules*, 1979, **12**, 980–988.
43 P. J. Flory and W. R. Krigbaum, *J. Chem. Phys.*, 1950, **18**, 1086–1094.
44 O. F. Olaj, W. Lantschbauer and K. H. Pelinka, *Macromolecules*, 1980, **13**, 299–302.
45 B. Kruger, L. Schäfer and A. Baumgärtner, *J. Phys.*, 1989, **50**, 3191–3222.
46 J. Dautenhahn and C. K. Hall, *Macromolecules*, 1994, **27**, 5399–5412.
47 C. N. Likos, M. Schmidt, H. Löwen, M. Ballauff, D. Pötschke and P. Lindner, *Macromolecules*, 2001, **34**, 2914–2920.
48 C. N. Likos, S. Rosenfeldt, N. Dingenouts, M. Ballauff, P. Lindner, N. Werner and F. Vögtle, *J. Chem. Phys.*, 2002, **117**, 1869–1877.
49 M. Bley, J. Dzubiella and A. Moncho-Jordá, *Soft Matter*, 2021, **17**, 7682–7696.
50 M. Bley, P. I. Hurtado, J. Dzubiella and A. Moncho-Jordá, *Soft Matter*, 2022, **18**, 397–411.
51 A. Moncho-Jordá, *Phys. Rev. Lett.*, 2020, **125**, 078001.
52 C. Miller, Y. Kim and J. Mittal, *Biophys. J.*, 2016, **111**, 28–37.
53 A. Scotti, A. R. Denton, M. Brugnoni, J. E. Houston, R. Schweins, I. I. Potemkin and W. Richtering, *Macromolecules*, 2019, **52**, 3995–4007.
54 A. Lang, C. N. Likos, M. Watzlawek and H. Löwen, *J. Phys.: Condens. Matter*, 2000, **12**, 5087.
55 S. Prestipino, F. Saija and P. V. Giaquinta, *Phys. Rev. E: Stat., Nonlinear, Soft Matter Phys.*, 2005, **71**, 050102.
56 A. Scotti, *Soft Matter*, 2021, **17**, 5548–5559.
57 H. Senff and W. Richtering, *J. Chem. Phys.*, 1999, **111**, 1705–1711.
58 M. Pelaez-Fernandez, A. Souslov, L. A. Lyon, P. M. Goldbart and A. Fernandez-Nieves, *Phys. Rev. Lett.*, 2015, **114**, 098303.
59 A. Scotti, U. Gasser, E. S. Herman, J. Han, A. Menzel, L. A. Lyon and A. Fernandez-Nieves, *Phys. Rev. E*, 2017, **96**, 032609.
60 K. Nothdurft, D. H. Müller, S. D. Mürtz, A. A. Meyer, L. P. B. Guerzoni, A. Jans, A. J. C. Kühne, L. De Laporte, T. Brands, A. Bardow and W. Richtering, *J. Phys. Chem. B*, 2021, **125**, 1503–1512.
61 G. D. Monte, D. Truzzolillo, F. Camerin, A. Ninarello, E. Chauveau, L. Tavagnacco, N. Gnan, L. Rovigatti, S. Sennato and E. Zaccarelli, *Proc. Natl. Acad. Sci. U. S. A.*, 2021, **118**, e2109560118.
62 R. Elancheliyan, G. Del Monte, E. Chauveau, S. Sennato, E. Zaccarelli and D. Truzzolillo, *Macromolecules*, 2022, **55**, 7526–7539.
63 M. R. R. Kannan, B. V. R. Tata, R. Dasgupta, S. Ahlawat and P. K. Gupta, *AIP Conf. Proc.*, 2011, **1391**, 359–362.
64 D. Karthickeyan, D. K. Gupta and B. V. R. Tata, *J. Opt.*, 2016, **18**, 105401.
65 Y. Hirokawa and T. Tanaka, *J. Chem. Phys.*, 1984, **81**, 6379–6380.
66 M. Annaka and T. Tanaka, *Nature*, 1992, **355**, 430–432.
67 P. Werner, M. Münzberg, R. Hass and O. Reich, *Anal. Bioanal. Chem.*, 2017, **409**, 807–819.
68 J. P. Baker and R. A. Siegel, *Macromol. Rapid Commun.*, 1996, **17**, 409–415.
69 S. Koga, S. Sasaki and H. Maeda, *J. Phys. Chem. B*, 2001, **105**, 4105–4110.
70 J. Gernandt and P. Hansson, *J. Phys. Chem. B*, 2015, **119**, 1717–1725.
71 G. M. Conley, P. Aebischer, S. Nöjd, P. Schurtenberger and F. Scheffold, *Sci. Adv.*, 2017, **3**, e1700969.
72 I. Bouhid de Aguiar, T. van de Laar, M. Meireles, A. Bouchoux, J. Sprakel and K. Schroën, *Sci. Rep.*, 2017, **7**, 10223.
73 A. Scotti, M. Brugnoni, A. A. Rudov, J. E. Houston, I. I. Potemkin and W. Richtering, *J. Chem. Phys.*, 2018, **148**, 174903.
74 J. Brijitta and P. Schurtenberger, *Curr. Opin. Colloid Interface Sci.*, 2019, **40**, 87–103.
75 M. Karg, A. Pich, T. Hellweg, T. Hoare, L. A. Lyon, J. J. Crassous, D. Suzuki, R. A. Gumerov, S. Schneider, I. I. Potemkin and W. Richtering, *Langmuir*, 2019, **35**, 6231–6255.
76 S. V. Nikolov, A. Fernandez-Nieves and A. Alexeev, *Proc. Natl. Acad. Sci. U. S. A.*, 2020, **117**, 27096–27103.
77 A. Scotti, M. F. Schulte, C. G. Lopez, J. J. Crassous, S. Bochenek and W. Richtering, *Chem. Rev.*, 2022, **122**, 11675–11700.
78 C. N. Likos, A. Lang, M. Watzlawek and H. Löwen, *Phys. Rev. E*, 2001, **63**, 031206.
79 C. N. Likos, B. M. Mladek, D. Gottwald and G. Kahl, *J. Chem. Phys.*, 2007, **126**, 224502.
80 C. N. Likos, B. M. Mladek, A. J. Moreno, D. Gottwald and G. Kahl, *Comput. Phys. Commun.*, 2008, **179**, 71–76.
81 D. Coslovich and A. Ikeda, *Soft Matter*, 2013, **9**, 6786–6795.

